Dominant Interannual and Decadal Variability of Winter Surface Air Temperature over Asia and the Surrounding Oceans

CHIHIRO MIYAZAKI

National Institute for Environmental Studies, Tsukuba, Japan

TETSUZO YASUNARI

Hydrospheric Atmospheric Research Center, Nagoya University, Nagoya, Japan

(Manuscript received 9 January 2007, in final form 9 July 2007)

ABSTRACT

To clarify the interannual variability of winter surface air temperature (SAT) over Asia and the surrounding oceans, the authors applied principal component analysis to normalized monthly SATs. The first mode represents the Asian north–south dipole pattern with a node over the Tibetan Plateau. This component has close relationships to the Arctic Oscillation and cold surge variability around Southeast Asia, showing decadal oscillation with signal changes in 1988 and 1997. The second mode is the inner-Asian mode with a center to the north of the Tibetan Plateau. This component connects to fluctuations of not only the western Siberian high but also the Icelandic low, which is associated with the pattern of the polar vortex over Eurasia. A recent warming trend and possible relationship to solar activity are also shown. The modes of Asian SAT variability associated with ENSO are extracted as the north–south dipole mode over the tropical western Pacific and Japan (the third mode) and Silk Road mode (the fourth mode). The two independent modes appear to be caused by different sea surface temperature (SST) anomalies over the western Pacific and Indian Ocean and their associated atmospheric Rossby wave responses: the atmospheric wave trains over both the north and south of the Tibetan Plateau in the third mode, and the atmospheric wave train that propagates toward the Silk Road via Greenland in the fourth mode.

1. Introduction

The global mean of surface air temperature (SAT) has increased by approximately 0.6°C since the late nineteenth century (Houghton et al. 2001). During this period, the largest warming (0.17°C decade^{-1}) has occurred since the late 1970s (Karl et al. 2000). Mid- and high-latitude regions of continental Asia have shown the strongest warming of the world, exceeding 0.6°C decade^{-1} (Wang and Gong 2000). The warming trend in mid- and high-latitude areas of Asia has occurred mainly in winter (Houghton et al. 2001; Yasunari et al. 1998).

However, few studies have examined the trend and interannual variability of the winter SAT in mid- and low-latitude areas of Asia. Gong and Ho (2004) investigated the temperature trend using station data for China and Korea from 1954 to 2000; their results indicated significant warming in northern China, while most stations south of 30°N experienced weaker warming trends. Yatagai and Yasunari (1994) also noted a warming trend in northern China north of 35°N, as well as a conspicuous cooling trend over Sichuan and Yunnan provinces from 1951 through 1994. By contrast, according to Houghton et al. (2001), based on data from 1976 to 2000, a warming trend exceeding 0.6°C decade^{-1} spreads over the South China Sea.

Warming trends are also found in the annual mean SAT in tropical Asia. Harger (1995) demonstrated a warming of 0.134°C decade^{-1} in Jakarta from 1866 to 1993. Malhi and Wright (2004) estimated the trend in Southeast Asia as 0.2°–0.3°C decade^{-1}. Given the small amplitude of temperature variations in the tropics, these values are noteworthy. In contrast, Kubota and Terao (2004) described a cooling trend since the last half of the 1970s in the interannual variation of the annual mean tropical tropospheric temperature.

Corresponding author address: Tetsuzo Yasunari, Hydrospheric Atmospheric Research Center, Nagoya University, Nagoya Furocho, Chikusa-ku, Nagoya 464-8601, Japan.
E-mail: yasunari@hyarc.nagoya-u.ac.jp

DOI: 10.1175/2007JCLI1845.1

Some of these temperature trends have been explained by associated climate periodic variabilities, in addition to the anthropogenic climate change. Many studies (e.g., Hurrell and van Loon 1997; Thompson and Wallace 1998) reported that the wintertime temperature variability in recent decades, especially the warming tendency in mid- and high-latitude Eurasia, is influenced by positive phase of the North Atlantic Oscillation (NAO)–Arctic Oscillation (AO). According to the analysis on the zonal-averaged atmospheric condition by Thompson and Lorenz (2004), this atmospheric fluctuation in middle and high latitude exerts the influence on the tropics.

Moreover, ENSO has undergone successive warm phase since about 1976 (Houghton et al. 2001). In general, the climate over Southeast Asia is warm and dry in the case of El Niño (e.g., Harger 1995; Malhi and Wright 2004). Hurrell (1996) showed that the warm phase of El Niño contributes to the warming over parts of Siberia and cooling over the North Pacific Ocean. Many studies agree that the warm phase of El Niño results in weak Asian winter monsoon (Horel and Wallace 1981; Tomita and Yasunari 1996).

Influence of solar cycle (especially 11-yr cycle) to the earth's climate has also been studied in various studies. Lassen and Friis-Christensen (1995) shows the strong correlation between the solar cycle length and the annual average temperature in Northern Hemisphere during the recent 120 yr. The solar effect on the lower and middle atmosphere in the objective analysis data (Gleisner and Thejll 2003) and global SST (Lohmann et al. 2004) are also reported.

In this paper, we extract the dominant spatiotemporal pattern of SAT variabilities during winter in the high latitudes through the tropics over the whole of Asia, and examine the associations of these patterns with atmospheric circulation, the winter monsoon, and other climate variables. The dominant spatial patterns of the SAT anomalies were obtained by empirical orthogonal function (EOF) analysis that is introduced in section 2. Section 3 describes the spatial and temporal characteristics of the dominant SAT modes. Section 4 presents the composite chart analysis of atmospheric circulation for each dominant mode, which was conducted to reveal the relationships between each mode and climate variables. The correlations of each mode with several relevant climate indices are also examined. We will draw the summary and some discussions in section 5.

2. Data and method of analysis

We have used monthly datasets of National Centers for Environmental Prediction–National Center for Atmospheric Research (NCEP–NCAR) reanalysis (version 1) data (Kalnay et al. 1996). Our period of interest is 1979/80–2002/03. We defined November–March (i.e., 120 months for the 24 yr) as winter season and employed near-surface air temperature at the 0.995 sigma level as SAT. The Asian region was defined as the rectangular area extended from 40° to 160°E and from 10°S to 70°N, which covers the entire area of the Siberian high, the area from northwestern India (Rao 1981) to East Asia influenced by the winter monsoon, and the area of cold surges from the western Pacific to Indian Ocean (Meehl et al. 1996). To estimate SAT variation in Asia from the low through high latitudes, normalized SAT anomaly data for each calendar month were produced using the average and standard deviation of 24 yr for each grid (2.5° × 2.5°).

We then applied EOF analysis to all the normalized monthly SAT data for Asia. Prior to this analysis, each grid value was weighted by the square root of the cosine of latitude to reflect the actual area of the individual grid. In our study, to extract dominant modes in the normalized SAT variation influencing over the whole of Asia and surrounding oceans covering high latitudes through low latitudes, we adopted the ordinary EOF analysis to them, and the results of first four components realistically showed regionalities for our analyzed area in winter. Thus, we did not think that we needed to adopt another analysis, such as rotated EOF analysis. Alternatively, to improve the robustness of this EOF analysis, we showed the original SAT variations at or near the positive and negative centers of action for each EOF mode.

We also compared the time coefficients for each principal component mode with several climatic indices: the Arctic Oscillation index (AOI), the Southern Oscillation index (SOI), and solar flux data (10.7 cm; F10.7) provided by the National Oceanic and Atmospheric Administration/Climate Prediction Center (NOAA/CPC); University of East Anglia/Climate Research Unit (UEA/CRU); and National Research Council, Canada, respectively. We have also employed the Siberian high index (SHI), as a measure of the Asian winter monsoon intensity that is presumed to be closely related to the winter SAT in Asia (e.g., Gong and Ho 2002; Panagiotopoulos et al. 2005). Following the method of Panagiotopoulos et al. (2005), we defined SHI to represent the average value of sea level pressure (SLP) averaged over the region extended from 40° to 60°N and 80° to 120°E. Additionally, Northern Hemisphere average temperature by the UEA/CRU (Jones and Moberg 2003) is referred to in the summary and discussion.

Composite charts for mode 1 of the SAT variability

TABLE 1. Percentages of variances and cumulative variances for the principal component mode of this study.

	Variance (%)	Cumulative variance (%)
EOF1	22.5	22.5
EOF2	15.3	37.8
EOF3	11.2	49.0
EOF4	9.1	58.1
EOF5	5.6	63.7
EOF6	5.3	68.9
EOF7	4.4	73.3
EOF8	3.3	76.6
EOF9	3.2	79.8
EOF10	2.6	82.3

were constructed by selecting months in which the time score of mode 1 >1 and those in which the score <-1. We repeated this procedure for the remaining modes. Climate variables considered for the composite chart analysis were SLP, surface wind, geopotential height, and wind at 200 hPa from NCEP–NCAR reanalysis data. In addition, NOAA Extended Reconstructed Sea Surface Temperature (SST) and Global Precipitation Climatology Project (GPCP) data were also used. To check if these composite fields are statistically significant, a t test is made by comparing with the average over all of the data period.

3. Principal modes of winter SAT anomalies over Asia and the western Pacific

In this section, we briefly describe the spatial–temporal characteristics of the major principal component modes.

Our analysis revealed that the four leading modes explain 22.5%, 15.3%, 11.2%, and 9.1%, respectively, of the variance and are well separated from the higher modes (Table 1), for which the criteria of North et al. (1982) were applied. For convenience, we will define 1) north–south dipole mode over Asia, 2) inner-Asian mode, 3) north–south dipole mode over the tropical western Pacific and Japan, and 4) Silk Road mode, to represent the four leading modes.

a. North–south dipole mode over Asia

Figure 1a shows the eigenvector spatial pattern of the first mode. The pattern represents a dipole SAT anomaly between Siberia and the South China Sea, with a node region near the Tibetan Plateau. Time series of this mode (Fig. 1b, top) primarily represented the interannual variation in SAT, because intraseasonal variability of this component within the 5-month scores of one winter was much smaller than that of other modes described later. In this figure, negative or slightly positive (less than +1) scores tended to appear from 1988/89 through 1996/97, implying dominant cold anomalies over the South China Sea and warm anomalies in Siberia. From 1997/98 through 2002/03, the time scores changed to positive or slightly negative values (more than -1), corresponding to warm anomalies over the South China Sea and cold anomalies over Siberia; that is, decadal-scale variation also dominated in this mode. These tendencies can be confirmed in the time series of normalized SAT at and near the centers of action of this mode (i.e., around the negative and positive extreme values of the eigenvectors over central Siberia and northern Philippines, respectively) as shown in Fig. 1b (bottom).

b. Inner-Asian mode

The spatial structure of the second mode exhibits a significant positive SAT anomaly north of the Tibetan Plateau (Fig. 2a). The core of the anomaly occurs along the arid/semiarid region of China, Mongolia, and central Asia; hence, we call this the inner-Asian mode. An anomaly that is less organized but of the same sign as in the inner-Asian region is present over the equatorial Indian Ocean and the Maritime Continent. In the corresponding time series (Fig. 2b, top), two successive negative phases appeared for 1979/80–1986/87 and 1991/92–1996/97, which reflected cold phases. By contrast, positive phases were also observed in the periods of 1987/88–1990/91 and 1997/98–2002/03, corresponding to warm phases. These temporal characteristics indicated that this mode had a decadal variation differing from that of the first mode. The score of this mode represents the SAT variation over the northern Tibet well, meanwhile the SAT fluctuation over equatorial Indian Ocean shows the decadal variation more clearly, especially from the late 1980s to the late 1990s (Fig. 2b, bottom). The second mode is also characterized by a remarkably positive linear trend ($+0.047\ \mathrm{yr}^{-1}$ of winter mean) which is significant at the 95% level; the other modes showed no significance. Considering the prominent positive tendency of the score since 1997/98, the recent warm anomaly was particularly prominent in this mode.

c. North–south dipole mode over the tropical western Pacific and Japan

The spatial pattern of the third mode is characterized by the largest positive and negative anomalies over the tropical western Pacific and southwestern Japan, respectively (Fig. 3a). Significant negative SAT anomaly is also found in the Arabian Sea. The time series of the score (Fig. 3b, top) are highly variable on interannual time scales. The extreme score values above +1 (e.g., 1983/84, 1985/86, and 1999/2000) and below -1 (e.g.,

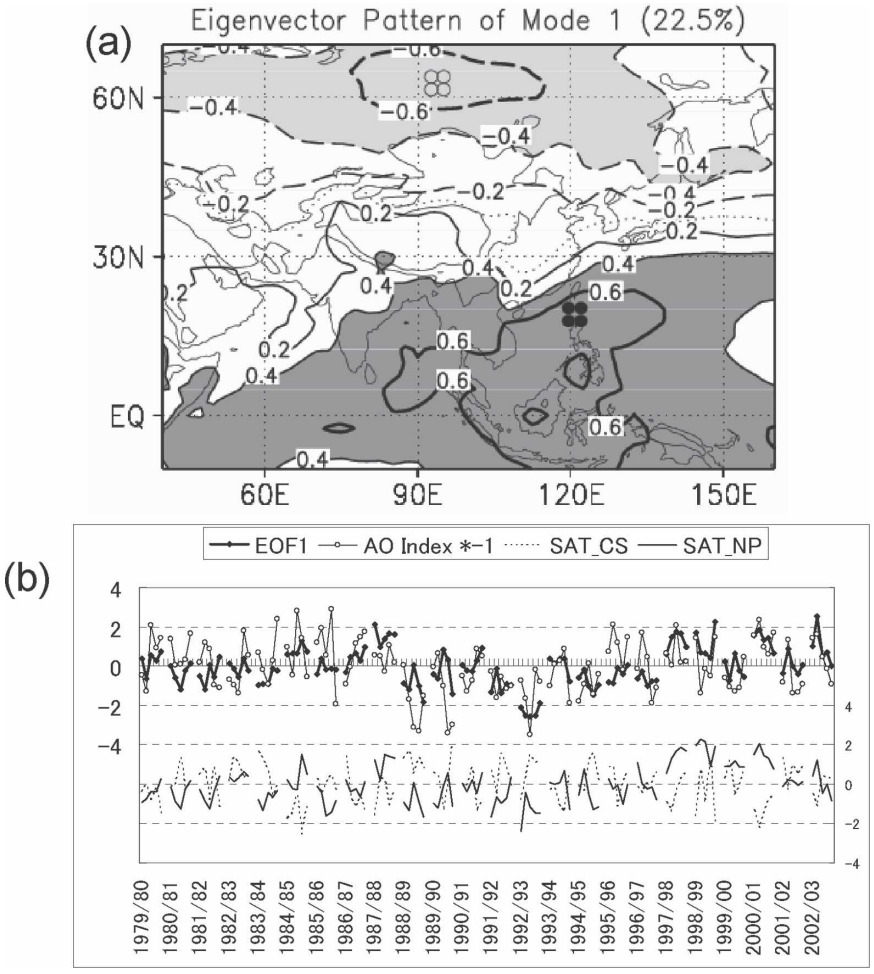

FIG. 1. The first component of normalized surface temperature anomalies in winters from 1979/80 to 2002/03. (a) Eigenvector patterns. Contour intervals (CIs) of 0.2. Solid (dashed) lines correspond to positive (negative) contours. The shaded area indicates coefficients $>$ ($<$) 0.4 (-0.4); 1000 and 3000 m altitudes are also shown. (b, top) Time series of the score (thick line); *Y*-axis is in the left side. Five scores of November through March are shown successively, as one winter. The AOI multiplied by -1 (thin line) is superimposed. See the main text (section 4a). (b, bottom) Time series of normalized SAT around the extreme value of the eigenvector. Solid (dashed) line is the average of four grids located in the positive (negative) area over northern Philippines (central Siberia), shown as closed (open) circles in (a); the *y* axis is on the right side.

1992/93, 1997/98) correspond to cold (warm) SAT over southern Japan and warm (cold) SAT over the western Pacific, respectively (Fig. 3b, bottom). In addition, SAT variation over the eastern Arabian Sea also shows in (out of) phase with that over southern Japan (the tropical western Pacific), which suggest that this mode is related to the ENSO over the tropical Pacific and Indian Ocean basins (as will be discussed in section 4c).

d. Silk Road mode

This mode exhibits a SAT anomaly along the northern periphery of the Tibetan Plateau (Fig. 4a). The negative anomaly has a center over the eastern plain area of the plateau, and extends over the northern through the western edges of the plateau, which corresponds to the ancient "Silk Road." The positive anomalies were located both in northern Eurasia (northward of 55°N) and the tropical oceans (Indian Ocean and the southern South China Sea). The time series (Fig. 4b, top) revealed the presence of extreme events: There are two extreme positive phases in 1982/83 and 1997/98; by contrast, extreme negative value is shown in 1998/99. These extreme positive (negative) values of the score are coincident with extremely warm (cold) SAT winters

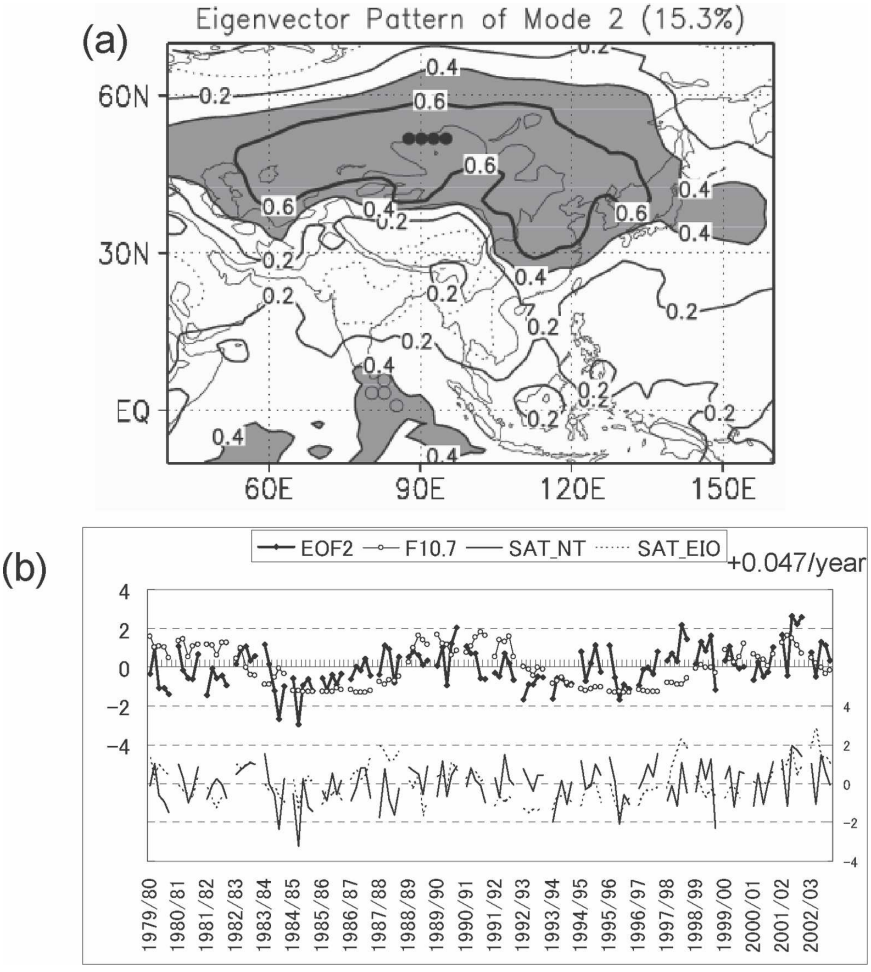

FIG. 2. Same as in Fig. 1, but for the second component. In the top of (b), F10.7 (thin line) is superimposed. In the bottom of (b), solid (dashed) line is the average of four grids located in the positive area over northern Tibet (equatorial Indian Ocean), shown as closed (open) circles in (a).

over the southern Indian Ocean and extremely cold (warm) SAT over eastern Tibet (Fig. 4b, bottom).

4. Atmospheric circulation patterns related to the four principal modes of SAT

In this section, we performed the composite charts analysis of climate variables to examine the anomalous circulation patterns associated with each mode. These charts (Figs. 5–8) show the synoptic pattern for the positive phase of each component time series. The climate variables used here are 1) SLP and surface wind, 2) geopotential height and wind at 200 hPa, 3) SST, and 4) precipitation. The analysis of the correlation between the four modes and three major climate variations (AOI, F10.7, and SOI) will be summarized in Table 2.

a. North–south dipole mode over Asia

A prominent, positive SLP anomaly is located over northern Eurasia and the Arctic, whereas the negative SLP anomaly is visible south of the Tibetan Plateau (Fig. 5a). Surface wind anomalies over and around Southeast Asia (i.e., southerly wind around the Philippines, cross-equatorial flow, anticyclonic circulation over the Philippine Sea, and easterly wind over the Malay Peninsula) indicates that the Asia north–south dipole mode, although extracted from monthly data, is likely connected with the weakening of cold surges in this area. At 200 hPa (Fig. 5b), the wind direction around the Philippine Islands is nearly opposite that at the surface, which is indicative of the local weakening of the Hadley cell, accompanied by cold surges.

In the positive (negative) composite chart of SST

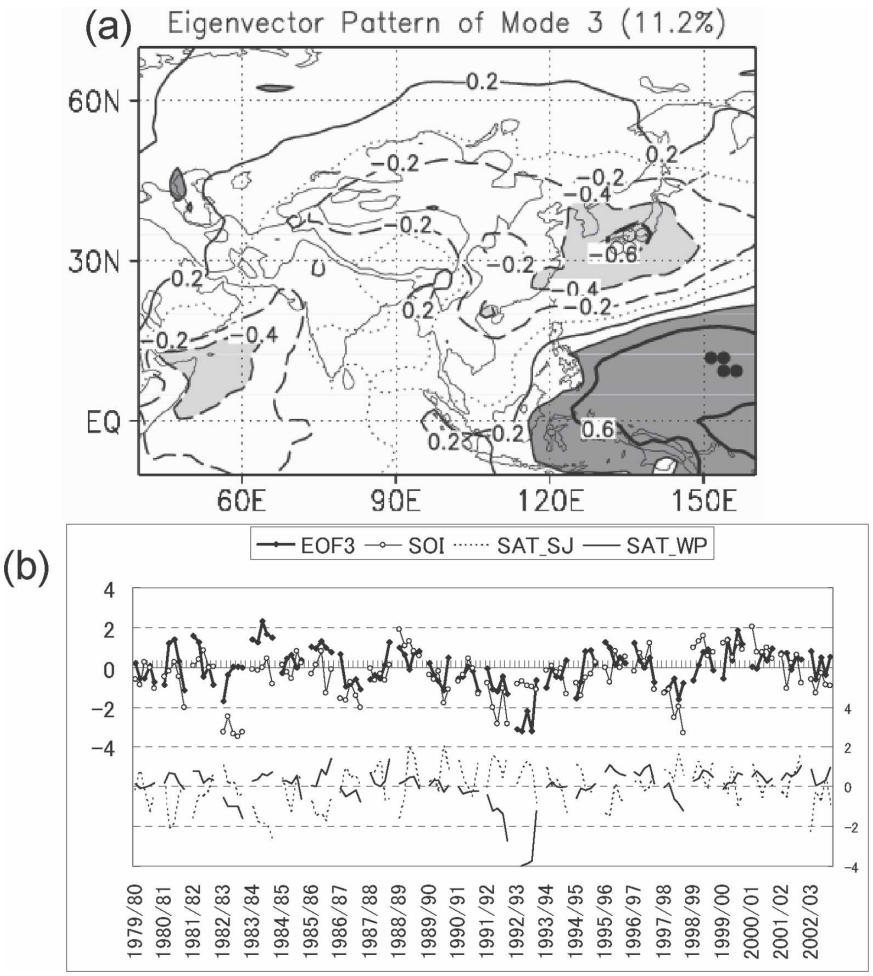

FIG. 3. Same as in Fig. 1, but for the third component. In the top of (b), the SOI (thin line) is superimposed. In the bottom of (b), solid (dashed) line is the average of four grids located in the positive (negative) area over the western Pacific (southern Japan), shown as closed (open) circles in (a).

anomalies on the first component (Fig. 5c), warm (cold) SST anomalies are located over the northwestern Pacific to the south of Japan, East China Sea, and South China Sea, where weaker (stronger) northeasterlies at the surface prevail, which are associated with the anomalous winter monsoon condition over East Asia (Fig. 5a). This spatial pattern of SST anomalies corresponds well with the anomalous sea surface condition of the winter monsoon over East and Southeast Asia through the control of the latent heat flux, as discussed by some previous papers (e.g., Tomita and Yasunari 1996; Zhang et al. 1997). The diabatic heating process over the winter monsoon surge in East Asia (Yanai and Tomita 1998) also showed that a cold surge anomaly in fact induced changes in the sensible and latent heating anomaly, which in turn changed SST anomalies of this particular ocean. We thus have concluded that SST anomalies in the East and South China Seas area may principally be the result of a cold surge anomaly from the continent.

Over the North Atlantic–European sector and the North Pacific, north–south dipole SLP anomalies are also prominent, but the polarity differs between the two basins. They appear to be associated with the strengthened/weakened storm track of the Aleutian/Icelandic lows, and vice versa. The dipole SLP anomaly in North Atlantic appears to be related to the North Atlantic Oscillation.

The atmospheric circulation at 200 hPa in this mode indicated the annular seesaw pattern of height between the Arctic and midlatitudes (Fig. 5b), which corresponded to the AO pattern reported by Thompson and Wallace (1998). In fact, the correlation coefficient between the first mode and the AOI was −0.47 (Table 2)—the high-

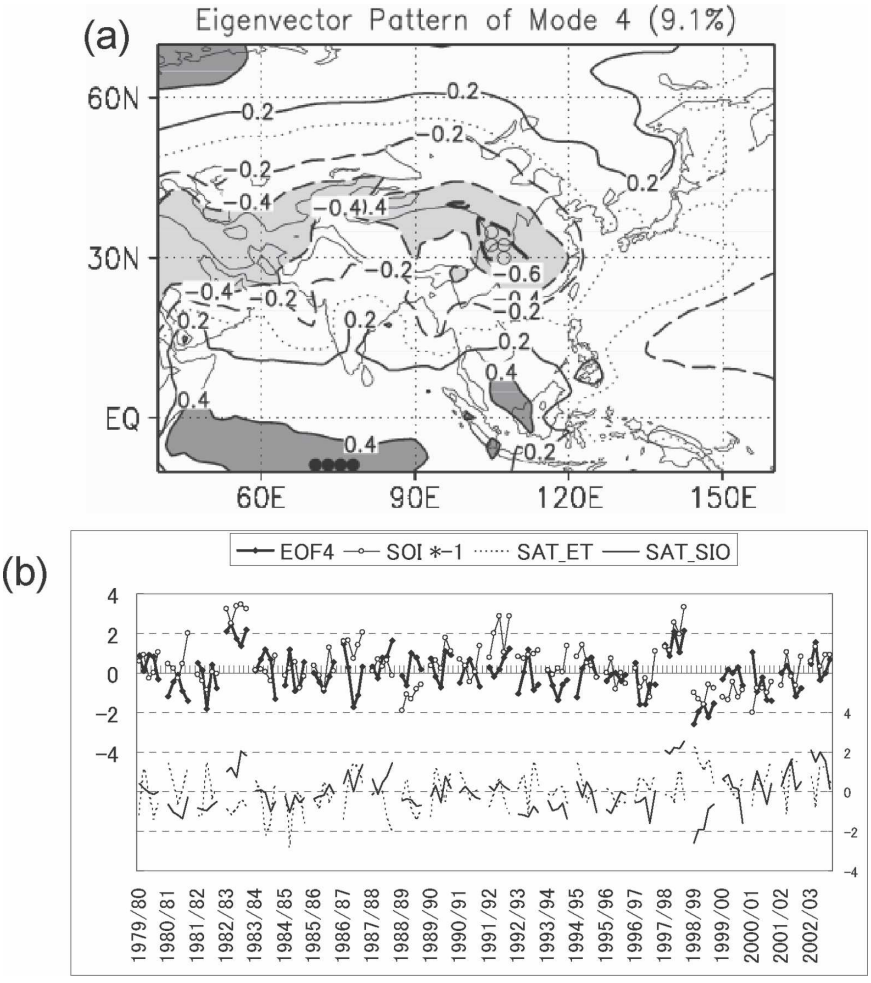

FIG. 4. Same as in Fig. 1, but for the fourth component. In the top of (b), the SOI multiplied by −1 (thin line) is superimposed. In the bottom of (b), solid (dashed) line is the average of four grids located in the positive (negative) area over the southern Indian Ocean (eastern Tibet), shown as closed (open) circles in (a).

est correlation among the four modes in this study. The AO appears to modulate the distribution of precipitation over the North Atlantic to central Siberia (Fig. 5d).

Therefore, we suggest that, to some extent, the Asian north–south dipole mode of the SAT anomaly is closely associated with the Arctic Oscillation that modulates fluctuation between the Icelandic low and the Aleutian low. It also modulates cold surge variability over Southeast Asia and the local Hadley circulation.

b. Inner-Asian mode

The second mode, inner-Asian mode, displays a huge cyclonic anomaly over western Eurasia in the composite chart of SLP and surface wind anomalies (Fig. 6a). The center of the anomaly is west of the Ural Mountains. As this mode is well correlated with SHI (−0.63, $p < 0.05$), it is a good proxy for the state of the cold wave north of 30°N in Asia. However, this cyclonic anomaly is indicative of not only weak westward expansion of the Siberian high, but also the strong Icelandic low in the case of a positive score. The positive precipitation anomaly over northwestern Eurasia (Fig. 6d) seems to be broadly consistent with this cyclonic anomaly.

Geopotential anomalies at 200 hPa (Fig. 6b) confirm not only the huge cyclonic anomaly over western Eurasia, but also the emergence of an anticyclonic anomaly to the north of the Tibetan Plateau. This pair of (north) west–(south) east anomalies over Eurasia indicated the pattern of the northern polar vortex that is characterized by the mean chart of upper geopotential height (not shown): tripole and dipole for positive and negative phases of the mode, respectively. Moreover, a pair of north–south height anomalies over East Asia links

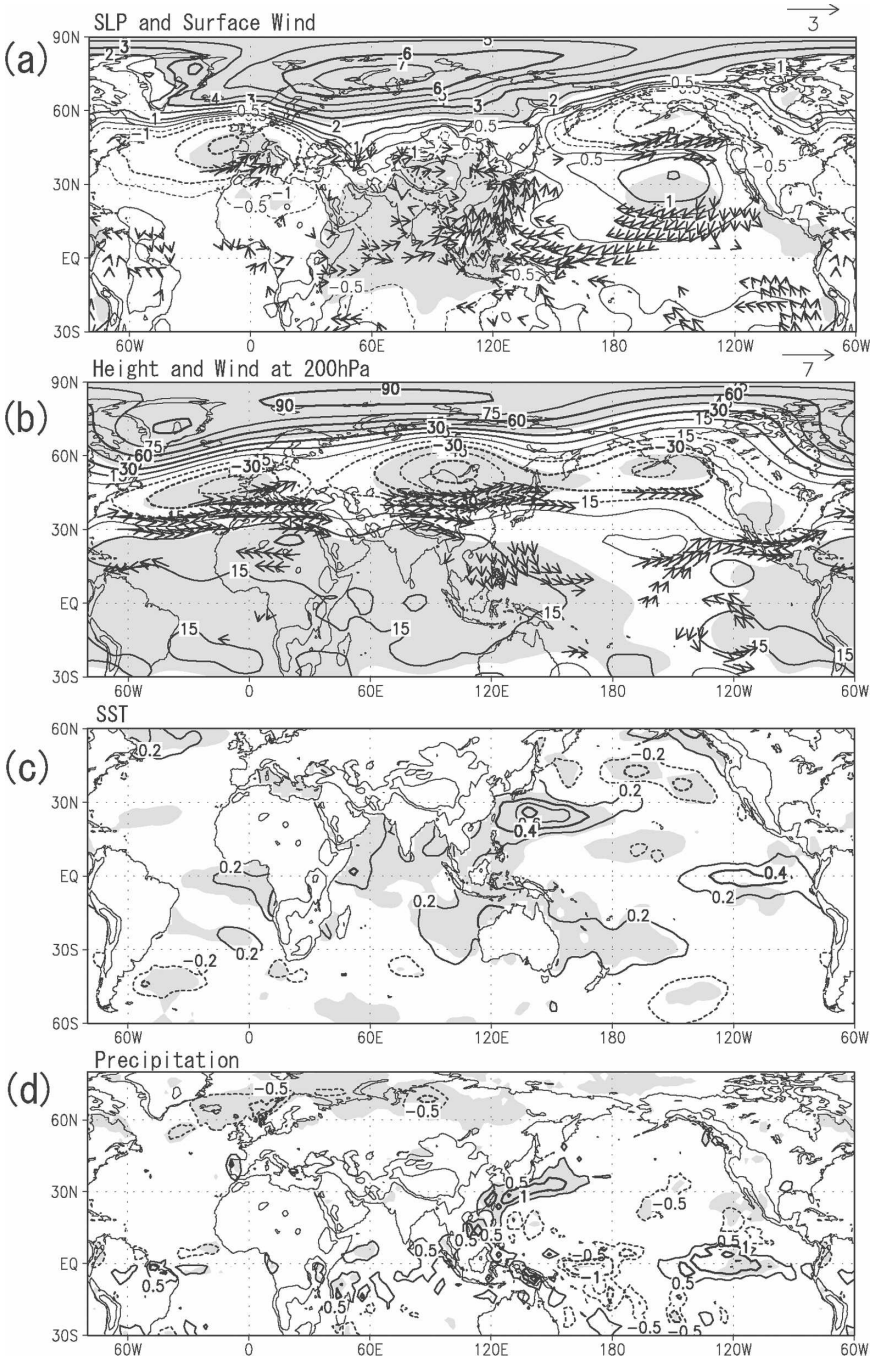

FIG. 5. Composite anomaly charts of the first component. Positive and negative anomalies are contoured by solid and dashed lines, respectively. (a) SLP and surface wind vector anomalies; CI is 0.5 hPa between −0.5 and 0.5 hPa, and otherwise is 1 hPa. (b) Geopotential height and wind vector anomalies at 200 hPa; CI is 15 m. (c) SST anomalies; CI is 0.2°C. (d) Precipitation anomaly; CI is 0.5 mm day^{-1}. The zero contour is omitted for SST and precipitation. Areas exceeding 5% significant t value are hatched. Wind vectors are only plotted (every 5°) where either the zonal or meridional component exceeds 5% significant t value.

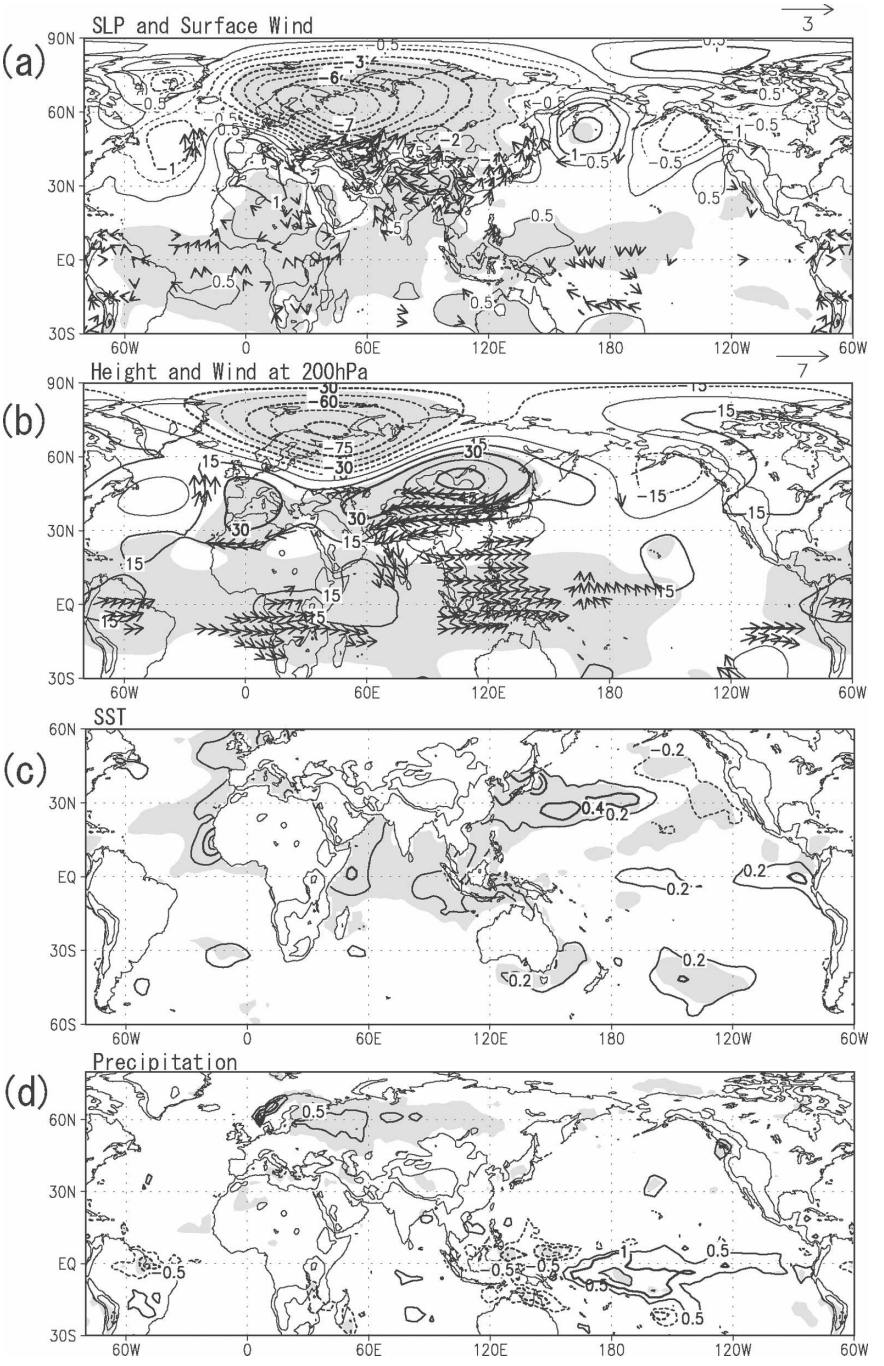

FIG. 6. Same as in Fig. 5, but for the second component.

the tropical zonal wind anomalies over the Maritime Continent.

Positive SST anomalies around Japan (Fig. 6c) may be induced by the weakening of surface westerly and SLP anomaly patterns over the latitudes (Fig. 6a), probably through a reduction in the surface latent heat fluxes to the atmosphere.

Therefore, this inner-Asian mode relates to the wax and wane of the western Siberian high and the shape of the polar vortex over northern Eurasia, which may be associated with the wave train pattern from northeast Europe toward Southeast Asia and the Maritime Continent.

Interestingly, this mode exhibits a linear warming

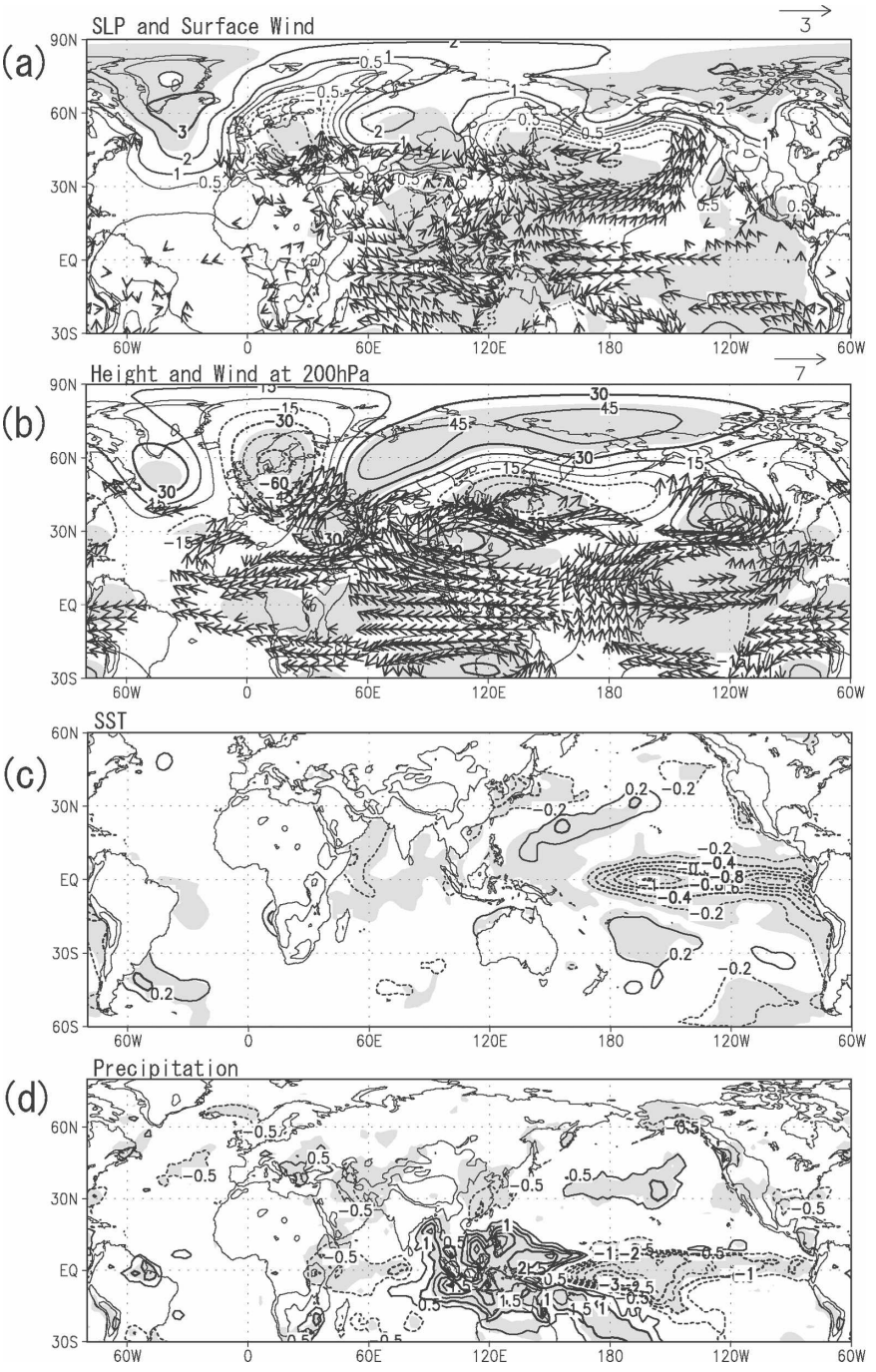

FIG. 7. Same as in Fig. 5, but for the third component.

trend, and also appears to be connected with the decadal-scale (approximately 11-yr cycle) solar activity. In fact, the SST anomaly of this mode was moderately correlated with the pattern influenced by the solar cycle (periodicity of 9–15 yr; see Lohmann et al. 2004). The correlation coefficient between this inner-Asian mode and F10.7 series was marginally significant (0.23; Table 2). Further discussion on the relation between this mode and the solar activity is attempted in section 5.

c. *North–south dipole mode over the tropical western Pacific and Japan*

This mode is characterized by a west–east contrast of the SLP anomaly over East Asia (Fig. 7a). This

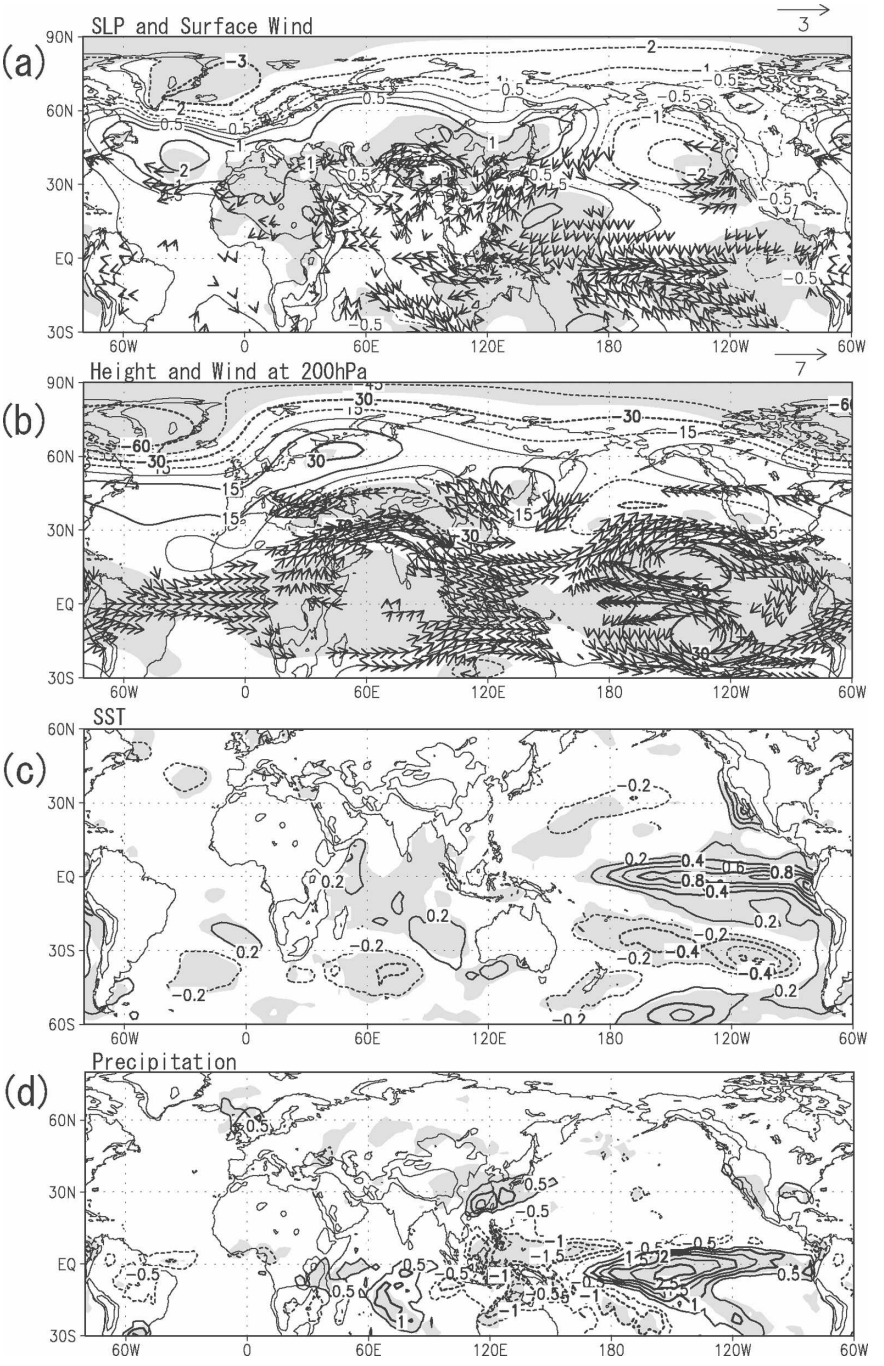

FIG. 8. Same as in Fig. 5, but for the fourth component.

anomaly appears to induce large temperature variations over Japan that are well correlated with the SST anomalies (Fig. 7c).

The composite map of circulation at 200 hPa (Fig. 7b) showed wave trains over much of Eurasia, through both the north and south of the Tibetan Plateau. The northern wave train contains the Eurasian (EU) and western Pacific (WP) patterns (Wallace and Gutzler 1981) over northern Eurasia. On the southern wave train, height anomalies over the Middle East and the southeastern edge of the Tibetan Plateau could modulate the strength of the subtropical jet. These two wave trains pass over Europe, and their origin could be tracked back westward to the tropical eastern Pacific. This tele-

TABLE 2. Correlation coefficients between the four principal component time series and some major climate indices. Boldface denotes that the probability values (p value) of the correlation coefficients are significant with the value below 0.05.

	EOF1	EOF2	EOF3	EOF4
AO	**−0.47**	**0.25**	−0.15	**0.22**
F10.7	−0.10	**0.23**	−0.04	0.04
SOI	0.04	−0.11	**0.44**	**−0.48**

connection pattern seems to be a standing Rossby wave train influenced by El Niño–Southern Oscillation (ENSO) as shown in Horel and Wallace (1981). It could be reasonable that the wave train splits into a high zonal wavenumber component that is deflected equatorward via the Middle East and a low zonal wavenumber component that propagates toward the higher latitudes over Siberia and then East Asia (Hoskins and Ambrizzi 1993). In fact, this mode is correlated with SOI (0.44; Table 2). However, some years with the significant score value of this third mode do not exactly coincide with those of SOI (Fig. 3b), presumably because this mode is more directly related to the SST anomaly over the western Pacific rather than the SST anomaly over central and eastern Pacific (i.e., principal ENSO domain), as described below.

In the tropics, remarkable Walker circulation and associated precipitation anomalies are shown (Figs. 7a,b,d). The SST composite chart for this component (Fig. 7c) denotes the anomaly located over the central–eastern equatorial Pacific, indicative of the connection with ENSO. An extreme value over the central equatorial Pacific is detached from the anomaly over the eastern area. Over the equatorial western Pacific, the opposite SST anomaly is also very significant, although the anomalous value is less than in the central–eastern Pacific. The extending of the Walker circulation to the equatorial Indian Ocean (Fig. 7b) appears to be induced by SST anomaly in the Arabian Sea (Fig. 7c) and the upper wave train south of the Tibetan Plateau.

Apart from the deep tropics, the anomalous precipitation patterns are also evident in southern China and the Middle East. These are attributed to ENSO (Zhang and Sumi 2002; Barlow et al. 2002).

We therefore suggest that the third mode is largely linked to ENSO. Over the entire Eurasian region, atmospheric wave trains over both the north and south of the Tibetan Plateau emerged through the stationary Rossby wave response to the SST anomaly over the tropical Pacific. The linkage of tropical SST and atmospheric circulation over the Indian Ocean and the western Pacific could contribute the maintenance of these wave trains over the entire Eurasian region.

d. Silk Road mode

Over the Silk Road, the SAT variation appears to be associated with the SLP anomaly and the opposite height anomaly at 200 hPa (Figs. 8a,b). This baroclinic structure seemed to represent local fluctuations in the southern edge of the Siberian high and upper trough/ridge north of Tibetan Plateau. However, the correlation coefficient between SHI and time series of the fourth mode are 0.20 ($p < 0.05$), which is the least significant of the four components in this study.

In the equatorial central–eastern Pacific, a prominent Matsuno–Gill-type circulation pattern (Matsuno 1966; Gill 1980) is seen at 200 hPa (Fig. 8b), suggesting a stationary response to the localized heating anomalies in this region. Its heating origin is the SST anomaly over the central–eastern Pacific (Fig. 8c), accompanied by ENSO. Walker-type anomalous zonal circulation was limited in the Pacific and Maritime Continent (Fig. 8b), differing from the third mode, which circulation extend to Indian Ocean. A pair of precipitation anomalies is located between the western Pacific and central–eastern Pacific (Fig. 8d), caused by ENSO and associated Walker circulation.

The other prominent atmospheric anomaly of this mode is located over Greenland (Figs. 8a,b), which appears to be linked to the Northern Atlantic Oscillation. We suggest that a Rossby wave train response to SST anomaly over the central–eastern equatorial Pacific propagates toward the Silk Road via Greenland.

Compared to the third mode, SST anomalies of this mode are characterized as follows: 1) The center of the anomaly is located over the central through eastern Pacific, 2) the anomaly over the western Pacific is less significant, and 3) significant SST anomalies of the Pacific and Indian Ocean are mainly located in the South Hemisphere. Particularly, the latter two characteristics of SST in this mode appear to cause the absence of the wave train south of the Tibetan Plateau, in contrast to the third mode. Moreover, these SST characteristics induce the features of precipitation in the Silk Road mode: 1) an anomaly over southern China, which is not accompanied with an anomaly over the Middle East; and 2) significant precipitation anomalies of the Pacific and Indian Oceans are mainly located in the Southern Hemisphere.

The correlation coefficients between SOI and this mode are significant (−0.48; Table 2). Differing from the third mode, the year with extreme values of this fourth mode tended to coincide with the year showing extreme values of SOI (Fig. 3b), because of its larger SST anomaly over the equatorial central–eastern Pacific.

Therefore, the Silk Road mode has a very clear dynamic link to ENSO. This mode corresponds to one component of Rossby wave train response by extremely large ENSO, which propagates toward the Silk Road via Greenland, rather than a local fluctuation of the southern Siberian high over the Silk Road.

5. Summary and discussion

We have examined the interannual and interdecadal variability of winter SAT over Asia and the surrounding oceans. Using principal component analysis of the normalized SAT for 24 winters, we have identified the four leading modes, namely: 1) north–south dipole mode over Asia, 2) inner-Asian mode, 3) north–south dipole mode over the tropical western Pacific and Japan, and 4) Silk Road mode. We have also constructed global composite maps of various climate variables for each mode.

Note that the first mode and the second mode are not so sensitive to the extent of EOF domain; an EOF analysis of interannual temperature anomalies over 50°–80°N, 80°–120°E (central Siberia) reveals the two leading modes comparable with those in this study (I. C. Handoh 2006, personal communication).

The north–south dipole mode over Asia is extracted as the first mode in Asia, which is associated with the atmospheric circulations of the Arctic Oscillation and cold surges in Southeast Asia.

The first mode shows some characteristics described in the previous studies on decadal oscillations: the North Atlantic Oscillation, the Arctic Oscillation, decadal climate shift, and so on. The northern center of action in the eigenvector pattern of the first mode extends to northern Japan (Fig. 1a), which is an important aspect of the North Atlantic Oscillation as pointed out by Xie et al. (1999). A composite map of SAT in the Northern Hemisphere (not shown) expresses the anomaly from northern Europe to Siberia and opposite anomalies over eastern Canada and northern Africa, which is an important feature of NAO. The SLP anomaly on the first mode also shows the anomalies of NAO (Fig. 5a). The correlation coefficient of this mode with the NAO index is quite significant (-0.25). On the other hand, the SAT over Japan except in northern Japan is more correlated with ENSO, as shown in the third mode (Fig. 3a), which is also described in Xie et al. (1999).

The temperature shift in 1988/89 northern winter shown in the score of the first mode is reported in the previous studies. Watanabe and Nitta (1999) concluded that the climatic shift is characterized as a dipole pattern of height anomalies between midlatitudes and polar regions with an equivalent barotropic structure. However, in their figure of SLP (their Fig. 1d), anomaly in the south of Tibetan Plateau (30°N, 90°E) is shown with the opposite sign to the higher latitude, which corresponds to the major surface anomaly associated with a cold surge in our first mode (Fig. 5a). In turn, our study has clarified that the dominant mode studied by Watanabe and Nitta (1999) for the high and midlatitudes is connected to lower latitudes in association with the Asian cold surges.

The linkage between the Arctic Oscillation and the tropical troposphere is consistent with previous studies. Over the northern and equatorial Atlantic, this regional linkage between the Arctic Oscillation and the tropics has been reported (e.g., Meehl and Van Loon 1979; McHugh and Rogers 2001). The dynamic mechanism of the zonal-mean tropical atmospheric circulation associated with Arctic Oscillation was demonstrated by Thompson and Lorenz (2004): forcing by waves originating at extratropical latitudes and the eddy momentum flux convergence at the tropics. Their paper showed a formation of the subtropical Hadley cell and a north–south temperature contrast near the surface, associated with the Arctic Oscillation (see their Fig. 1, top). These characteristics are consistent with the features in the composite charts of the first mode in the present study. In the case of Asia and the surrounding oceans, the variability of this regional Hadley cell links directly to the appearance/absence of cold surges in Southeast Asia. Therefore, the wax and wane of the Arctic Oscillation is most likely associated with the modulation of cold surges in Southeast Asia, through its regional Hadley cell over the eastern half of Eurasia.

Chang et al. (2004) indicated that only winter precipitation in the vicinity of Sumatra and the Malay Peninsula showed a weak relationship to ENSO; they concluded that the effect of ENSO was shut out by high mountains and variation of the cross-equatorial flow. In our study, the first mode showed close association with anomalous precipitation over the Malay Peninsula. Only this mode demonstrated the fluctuation of cross-equatorial wind accompanied with cold surges in Southeast Asia. Because this first mode showed close association with the Arctic Oscillation on decadal scales, the long-term variation of cold surges and precipitation in Southeast Asia should be studied in conjunction with the SAT and circulation changes of the higher latitudes, as well as the atmosphere–ocean system in the tropics.

Furthermore, atmospheric circulation of the first mode showed not only the direct relevance to North Atlantic Oscillation, but also the seesaw-like fluctuation between the Icelandic low and the Aleutian low. Honda and Nakamura (2001) investigated the process of late-winter formation of an interannual seesaw be-

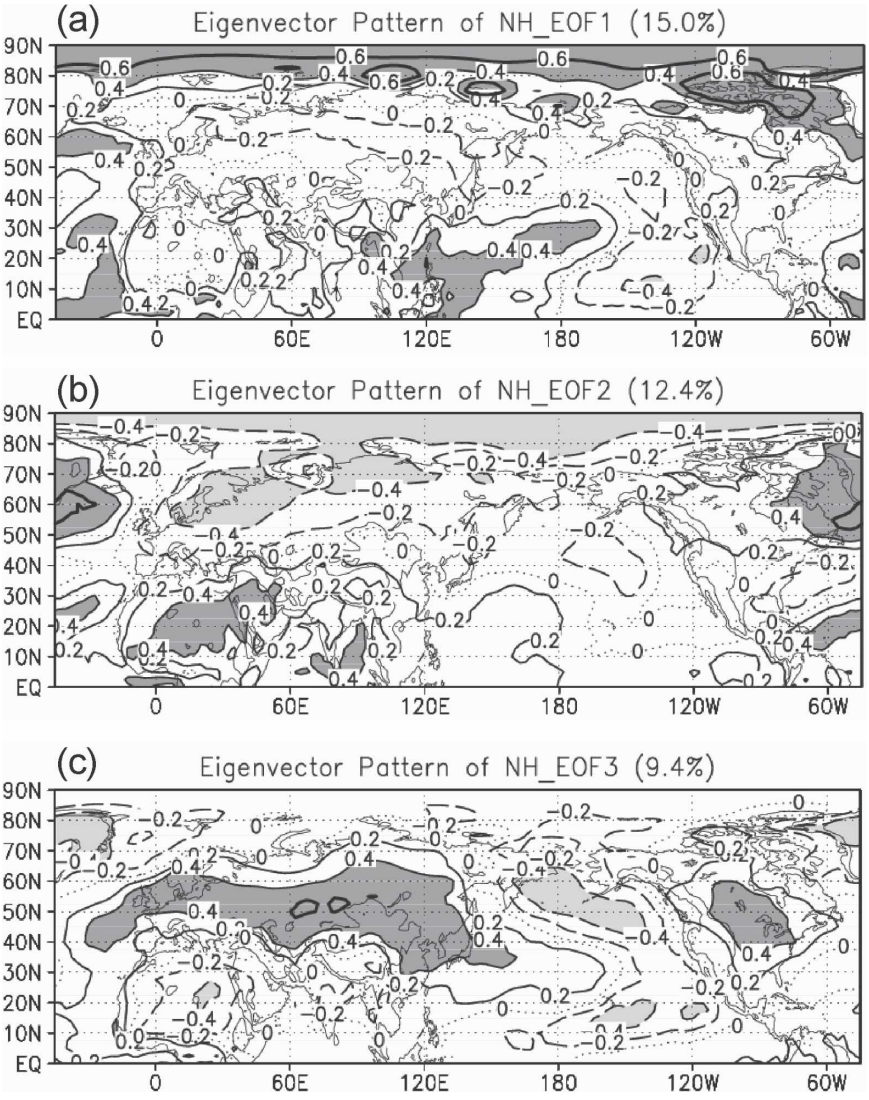

FIG. 9. Eigenvector patterns of the EOF analysis for normalized surface temperature anomalies in the Northern Hemisphere in winters from 1979/80 to 2002/03. (a) The first mode, (b) the second mode, and (c) the third mode are shown. Details for drawing are same as Fig. 1a.

tween the surface Aleutian and Icelandic lows, interpreting the Arctic Oscillation as the North Atlantic Oscillation in early winter and as the Aleutian–Iceland seesaw in late winter. The first mode of this study seemed to contain their circulation characteristics from early winter through late winter.

Inner-Asian mode, with a unique warming trend in Asia, is extracted as the second mode. This component indicated a significant correlation with Jones and Moberg's (2003) Northern Hemisphere average temperature (0.74, $p < 0.05$). This is likely to reflect that inner Asia is the region that shows one of the strongest global warming signals. Moreover, this inner-Asian mode showed the some relation with the solar cycle. Kodera (2002, 2003) pointed out that atmospheric feature of NAO was modulated by the solar cycle and the influence was shown in the anomaly of SLP and SAT over Eurasia. Furthermore, these studies showed that the feature over Eurasia connected to zonal wind in the troposphere through stratosphere. Hence, it should be clarified whether this significant correlation between the inner-Asian mode and solar activity is due to the fact that the huge mass of the Eurasian continent, which occupies a major terrestrial part in the Northern Hemisphere, may take a direct or indirect connection with the solar activity. For this issue, we thought that the

result of EOF analysis for normalized SAT in the Northern Hemisphere may prove the hemispheric extent of inner-Asian mode and its temporal tendency of appearance. As a result (Fig. 9), the synchronizing continental SAT mode over midlatitude Eurasia and America was extracted as the third mode (9.4%), following the synchronizing maritime mode in the Atlantic, western Pacific, and Arctic Oceans (EOF1: 15.0%) and NAO mode (EOF2: 12.4%). Temporal variation of this EOF3 in the Northern Hemisphere is almost the same as that of the second mode in Asia (correlation coefficient: 0.71), and shows better correlation with F10.7 (0.27). Therefore, this inner-Asian mode takes one part as hemispheric warming and as the huge mass of the Northern Hemisphere for a direct or indirect heating/cooling in conjunction with the solar activity. Further evidence and the mechanism of the connection between the second component and the solar cycle will be examined separately, with reference to the theory on the indirect connection of solar activity with the earth's atmosphere through stratospheric (ozone) circulation, as shown in Kodera and Kuroda (2002).

The modes of Asian SAT variability associated with ENSO are extracted as the north–south dipole mode over the tropical western Pacific and Japan (the third mode) and Silk Road mode (the fourth mode). The two independent modes were caused by respective remote Rossby wave responses to different sea temperature anomalies over the Pacific and Indian Oceans (in sections 4c and 4d). The two kinds of the Rossby wave response may cause the difference of precipitation variability in midlatitude Asia. The variation of precipitation in southern China was seen both in the third and the fourth modes, whereas the precipitation anomaly over the Middle East appeared only in the third mode. Zhang and Sumi (2002) concluded that precipitation variability in southern China was caused by a low-level circulation anomaly to the north of the Maritime Continent, which was forced through a Rossby wave train by the western tropical Pacific SST associated with ENSO. Since these characteristics are prominent over the Pacific in the case of typical ENSO, both the third and fourth modes contain this variability in southern China. On the anomalous precipitation in the Middle East, Barlow et al. (2002) pointed out the following three synoptic characteristics: the out-of-phase relationship of precipitation is prominent between the eastern Indian Ocean and the Middle East, this relationship is due to ENSO with a strong SST signal over the western Pacific, and anticyclonic circulations over the southeastern edge of the Tibetan Plateau and the Middle East are induced by strong convection over the eastern Indian Ocean and the western Pacific through a stationary Rossby wave response. A strong SST signal over the western Pacific and a remarkable anomaly of precipitation over the Indian Ocean correspond well to the features of the third mode. The precipitation variability in the Middle East can prove the robustness of the Rossby wave response to the western Pacific and Indian Ocean in the third mode.

To better understand and quantify the nature of Asian climate variability, further investigations into the dynamic and thermodynamic feedbacks operating in each climate mode are merited.

Acknowledgments. The NCEP–NCAR reanalysis datasets and NOAA extended reconstructed sea surface temperature were obtained from the Climate Diagnostics Center. Precipitation data of the Global Precipitation Climatology Project were obtained from the National Climatic Data Center. We thank Dr. Shinjiro Kanae (University of Tokyo), Dr. Akiyo Yatagai [Research Institute for Humanity and Nature (RIHN)], and Dr. Itsuki C. Handoh (Ehime University) for constructive comments and encouragement, which helped us to improve the manuscript. Chihiro Miyazaki was financially supported by a RIHN Project 5-1, Global Water Cycle Variation and the Current World Water Resources Issues and Their Perspectives.

REFERENCES

Barlow, M., H. Cullen, and B. Lyon, 2002: Drought in Central and Southeast Asia: La Niña, the warm pool, and Indian Ocean precipitation. *J. Climate,* **15,** 697–700.

Chang, C. P., Z. Wang, J. Ju, and T. Li, 2004: On the relationship between western maritime continent monsoon rainfall and ENSO during northern winter. *J. Climate,* **17,** 665–672.

Gill, A. E., 1980: Some simple solutions for heat-induced tropical circulation. *Quart. J. Roy. Meteor. Soc.,* **106,** 447–462.

Gleisner, H., and P. Thejll, 2003: Patterns of tropospheric response to solar variability. *Geophys. Res. Lett.,* **30,** 1711, doi:10.1029/2003GL017129.

Gong, D. Y., and C. H. Ho, 2002: The Siberian High and climate change over middle to high latitude Asia. *Theor. Appl. Climatol.,* **72,** 1–9.

——, and ——, 2004: Intra-seasonal variability of wintertime temperature over East Asia. *Int. J. Climatol.,* **24,** 131–144.

Harger, J. R. E., 1995: Air-temperature variations and ENSO effects in Indonesia, the Philippines and El Salvador. ENSO patterns and changes from 1866–1993. *Atmos. Environ.,* **29,** 1919–1942.

Honda, M., and H. Nakamura, 2001: Interannual seesaw between the Aleutian and Icelandic lows. Part II: Its significance in the interannual variability over the wintertime Northern Hemisphere. *J. Climate,* **14,** 4512–4529.

Horel, J. D., and J. M. Wallace, 1981: Planetary-scale atmospheric phenomena associated with the Southern Oscillation. *Mon. Wea. Rev.,* **109,** 813–829.

Hoskins, B. J., and T. Ambrizzi, 1993: Rossby wave propagation

on a realistic longitudinally varying flow. *J. Atmos. Sci.,* **50,** 1661–1671.

Hurrell, J. W., 1996: Influence of variations in extratropical wintertime teleconnections on Northern Hemisphere temperature. *Geophys. Res. Lett.,* **23,** 665–668.

——, and H. van Loon, 1997: Decadal variations in climate associated with the North Atlantic Oscillation. *Climatic Change,* **36,** 301–326.

Houghton, J. T., Y. Ding, D. J. Griggs, M. Noguer, P. J. van der Linden, X. Dai, K. Maskell, and C. A. Johnson, Eds., 2001: *Climate Change 2001: The Scientific Basis*. Cambridge University Press, 881 pp.

Jones, P. D., and A. Moberg, 2003: Hemispheric and large-scale surface air temperature variations: An extensive revision and an update to 2001. *J. Climate,* **16,** 206–223.

Kalnay, E., and Coauthors, 1996: The NCEP/NCAR 40-Year Reanalysis Project. *Bull. Amer. Meteor. Soc.,* **77,** 437–471.

Karl, T. R., R. W. Knight, and B. Baker, 2000: The record breaking global temperatures of 1997 and 1998: Evidence for an increase in the rate of global warming. *Geophys. Res. Lett.,* **27,** 719–722.

Kodera, K., 2002: Solar cycle modulation of the North Atlantic Oscillation: Implication in the spatial structure of the NAO. *Geophys. Res. Lett.,* **29,** 1281, doi:10.1029/2001GL014557.

——, 2003: Solar influence on the spatial structure of the NAO during the winter 1900–1999. *Geophys. Res. Lett.,* **30,** 1175, doi:10.1029/2002GL016584.

——, and Y. Kuroda, 2002: Dynamical response to the solar cycle. *J. Geophys. Res.,* **107,** 4749, doi:10.1029/2002JD002224.

Kubota, T., and T. Terao, 2004: Interdecadal variability of the seasonal-scale persistence in the tropical mean tropospheric temperature. *J. Meteor. Soc. Japan,* **82,** 1213–1221.

Lassen, K., and E. Friis-Christensen, 1995: Variability of the solar cycle length during the past five centuries and the apparent association with terrestrial climate. *J. Atmos. Solar-Terr. Phys.,* **57,** 835–845.

Lohmann, G., N. Rimbu, and M. Dima, 2004: Climate signature of solar irradiance variations: Analysis of long-term instrumental, historical, and proxy data. *Int. J. Climatol.,* **24,** 1045–1056.

Malhi, Y., and J. Wright, 2004: Spatial patterns and recent trends in the climate of tropical rainforest regions. *Philos. Trans. Roy. Soc. London,* **359,** 311–329.

Matsuno, T., 1966: Quasi-geostrophic motions in the equatorial area. *J. Meteor. Soc. Japan,* **44,** 25–43.

McHugh, M. J., and J. C. Rogers, 2001: North Atlantic Oscillation influence on precipitation variability around the Southeast African convergence zone. *J. Climate,* **14,** 3631–3642.

Meehl, G. A., and H. Van Loon, 1979: The seesaw in winter temperatures between Greenland and Northern Europe. Part III: Teleconnections with lower latitudes. *Mon. Wea. Rev.,* **107,** 1095–1106.

——, G. N. Kiladis, K. M. Weickmann, M. Wheeler, D. S. Gutzler, and G. P. Compo, 1996: Modulation of equatorial subseasonal convective episodes by tropical–extratropical interaction in the Indian and Pacific Ocean regions. *J. Geophys. Res.,* **101,** 15 033–15 049.

North, G. R., T. L. Bell, R. F. Cahalan, and F. J. Moeng, 1982: Sampling errors in the estimation of empirical orthogonal functions. *Mon. Wea. Rev.,* **110,** 699–706.

Panagiotopoulos, F., M. Shahgedanova, A. Hannachi, and D. B. Stephenson, 2005: Observed trends and teleconnections of the Siberian High: A recently declining center of action. *J. Climate,* **18,** 1411–1422.

Rao, Y. P., 1981: The climate of the Indian subcontinent. *World Survey of Climatology,* K. Takahashi and H. Arakawa, Eds., Vol. 9, *Climates of Southern and Western Asia,* Elsevier Scientific Publishing Company, 67–182.

Thompson, D. W. J., and J. M. Wallace, 1998: The Arctic Oscillation signature in the wintertime geopotential height and temperature fields. *Geophys. Res. Lett.,* **25,** 1297–1300.

——, and D. J. Lorenz, 2004: The signature and the annual modes in the tropical troposphere. *J. Climate,* **17,** 4330–4342.

Tomita, T., and T. Yasunari, 1996: Role of the northeast winter monsoon on the biennial oscillation of the ENSO/Monsoon system. *J. Meteor. Soc. Japan,* **74,** 399–413.

Wallace, J. M., and D. S. Gutzler, 1981: Teleconnections in the geopotential height field during the Northern Hemisphere winter. *Mon. Wea. Rev.,* **109,** 784–812.

Wang, S., and D. Gong, 2000: Enhancement of the warming trend in China. *Geophys. Res. Lett.,* **27,** 2581–2584.

Watanabe, M., and T. Nitta, 1999: Decadal changes in the atmospheric circulation and associated surface climate variations in the Northern Hemisphere winter. *J. Climate,* **12,** 494–510.

Xie, S. P., H. Noguchi, and S. Matsumura, 1999: A hemispheric-scale quasi-decadal oscillation and its signature in Northern Japan. *J. Meteor. Soc. Japan,* **77,** 573–582.

Yanai, M., and T. Tomita, 1998: Seasonal and interannual variability of atmospheric heat sources and moisture sinks as determined from NCEP–NCAR reanalysis. *J. Climate,* **11,** 463–482.

Yasunari, T., M. Nishimori, and T. Mito, 1998: Trends and interdecadal variations of the surface and lower-tropospheric temperature in the Northern Hemisphere from 1964 to 93. *J. Meteor. Soc. Japan,* **76,** 517–531.

Yatagai, A., and T. Yasunari, 1994: Trends and decadal-scale fluctuation of surface air temperature and precipitation over China and Mongolia during the recent 40 year period (1951–90). *J. Meteor. Soc. Japan,* **72,** 937–957.

Zhang, R., and A. Sumi, 2002: Moisture circulation over East Asia during El Niño episode in northern winter, spring and autumn. *J. Meteor. Soc. Japan,* **80,** 213–227.

Zhang, Y., K. R. Sperber, and J. S. Boyle, 1997: Climatology and interannual variation of the East Asian Winter Monsoon: Results from the 1979–95 NCEP/NCAR reanalysis. *Mon. Wea. Rev.,* **125,** 2605–2619.